Supporting Information

for

Differential toxicity of anatase and rutile TiO_2 nanoparticles to the antioxidant enzyme system and metabolic activities of freshwater biofilms based on microelectrodes and fluorescence in situ hybridization

Peifang Wang[a,b], Kun Li[a,b], Jin Qian[a,b*], Chao Wang[a,b], Bianhe Lu[a,b], Xin Tian[a,b], Wen Jin[a,b], Xixian He [a,b]

[a] Key Laboratory of Integrated Regulation and Resource Development on Shallow Lakes, Ministry of Education, Hohai University, Nanjing, People's Republic of China, 210098

[b] College of Environment, Hohai University, Nanjing, People's Republic of China, 210098

***Corresponding authors:**

Jin Qian, phone: 86-25-8378-7332; fax: 86-25-8378-7332;

E-mail: hhuqj@hhu.edu.cn

This Supporting Information includes a total of 22 pages (including this page) with 6 sections for text, 8 figures and 3 tables, references.

Test. S1. Colonization of freshwater biofilms and indoor training

In early summer, biofilms were cultivated in spherical bio-fillers with a diameter and specific surface area of 150 mm and 800 m^2/m^3, respectively. The bio-filters were made of polyethylene and were suspended in a freshwater lake (Fig. S1) (Taihu Lake, China, 31.3794 N, 120.0249 E) in rows to act as supports for phototrophic biofilms attachment. The content of titanium (Ti^{4+}) in this lake is very low (3.5±0.4 μg L^{-1}), suggesting that the communities were not pre-selected for titanium tolerance, because it seems reasonable to conduct a mechanistic study in term of the toxicity of nanoparticles by indoor culture, domestication of biofilms from freshwater systems and final exposure by controlling variables.[1,2] The physicochemical and nutritional parameters of this body of water are listed in Table S1. After incubating for 3 weeks, inocula were obtained by introducing aliquots of carriers and cultivated in flow cells at 20±1°C with a constant water flow. Briefly, the nutrient solution (Table S2), which was completely replaced four times a week to avoid nutrient depletion, was supplied from a 10-L plastic barrel located at the end of each flow cell and was recirculated at a rate of 100 mL min^{-1} through precision peristaltic pumps in case of the highly complex variability of natural water. Simultaneously, in order to provide a steady natural light source with a day and night rhythm of approximately 12-h:12-h to meet the requirements for normal growth and metabolism of the biofilms, two fluorescent lamps (CLEO Compact 25W−S-R, Philips, Germany) and 1 daylight lamp (BIOLUX, L 15W/72, Osram, Switzerland) were properly installed and adjusted to set the radiation intensity to UVA 3.6 mW cm^{-2},

UVB 0.19 mW cm^{-2}, and PAR 75 μE $m^{-2}s^{-1}$, which represents environmentally realistic UV irradiation reaching the water surface for a summer day.[3] During the culturing period, biofilms were sampled for exposure experiments until the dry biomass did not increase after this time point.[4]

Test. S2. Aggregation of TiO_2-NPs in the exposure suspension

Prior to the experiment, the aggregation kinetics of An-NPs and Ru-NPs in the filtered lake-water (through 0.22 μm) were investigated to study the stability of added NPs in freshwater environment. According to previous preliminary test, concentration of 10 mg L^{-1} NPs was used to provide a good detection and the particle-size distributions (PSD) of the NPs were measured by dynamic light scattering (DLS) using Malvern Zetasizer Nano ZSP. The homo-aggregation experiments of NPs suspensions were performed following the detailed procedure reported in previous study,[5] and the particle size distributions and zeta potentials of NPs in the solution were determined. Due to the low level of suspended solids (<0.05 mg L^{-1}) in the static biofilms incubation systems, the hetero-aggregation processes (aggregation between nanoparticles and suspended particles in the water column) in the microcosms were not taken consideration in this study.

As shown in Fig. S4, both the two types of TiO_2-NPs aggregated significantly ($p<0.05$) in the first 30 min, with hydrodynamic diameter (HDD) increased from 94 nm (An-NPs) and 193 nm (Ru-NPs) to approximate 1054 nm and 632 nm in the water column, respectively. The nano-aggregates were captured by SEM analysis and shown

in Fig. S4. The zeta potentials of two TiO_2-NPs were determined to be -23.3±0.6 mV (An-NPs) and -38.4±1.7 mV (Ru-NPs), respectively. Lower value of zeta potential of An-NPs indicated weak electrostatic repulsion between the nanoparticles,[5] resulting in more obvious aggregation of An-NPs in the lake-water compared to that of Ru-NPs. In addition, the more stable Ru-NPs in lake-water might be attributed to the fact that pH_{zpc} values (4.1) (Fig. S3, zeta potentials <−30 mV) of Ru-NPs is farther away from the pH (7.26) of lake-water compared to that of An-NPs.[6] Moreover, the obvious aggregation processes of both TiO_2-NPs might be due to the acceleration of the high ionic strength, dissolved salts and dissolved organic matter present in the lake-water (Table S1).[7, 8] Realistically, when NPs were released to freshwater systems, homo-aggregation might not be the only mechanisms of NPs colloidal destabilization and hetero-aggregation might occur with the presence of natural colloids in the microcosms.[9]

Test. S3. Viability assessment assays

Definition of bacterial cells death modes (NLD and ALD)

Here, intact cells are those with membrane integrity, which demonstrates the protection of constituents in intact cells classified as viable cells. Cells without an intact membrane are considered as permeabilised and can be classified as necrosis-like death (NLD) indicating cells have severe inflammatory reactions and permeabilized cytoplasmatic-membrane with cytoplasmic leakage,[10, 11] while in addition to the cells shrinkage without inflammation and eventually release phage-like particles like apoptotic bodies with membrane integrity,[11, 12] apoptosis-like-death (ALD) also shows

the expression of a bacterial protein with affinity for caspase substrate peptides.[13]

Multi-color fluorescence flow cytometry

The fluorochromes Propidium Iodide (PI, λ_{ex} =535 nm, λ_{em} =617 nm) and SYBR Green I (SGI， λ_{ex} =495 nm, λ_{em} =525 nm) are widely reported as high-affinity nucleic acid dyes capable to give bright staining of the cells.[14, 15] SGI, a membrane permeable dye, can be combined with nucleic acid of viable and dead cells with the excitation wavelength of green dye, while PI, a without membrane permeability dye, could not penetrate the living cell membrane, once the membrane becomes damaged to an extent that some PI is able to enter the cell (namely the NLD according to our past study[11]), PI binds to DNA and the red fluorescence increases. That is to say, in NLD cells, the presence of both dyes activates the fluorescence resonance energy transfer phenomenon (FRET) so that green fluorescence emission of SGI is no longer visible; thus NLD cells appear only as red fluorescent, while intact cells appear as green fluorescent. A 1: 1000 (v/v) dilution of the SGI (10,000× stock; Invitrogen) commercial stock solution was made in dimethyl sulfoxide (DMSO). The PI commercial stock solution has a concentration of 1 mg mL^{-1}. Staining with SGI and PI was made adding 20μL of both fluorochromes for each 100μL of sample with a concentration about 1×10^6~1×10^7 cells mL^{-1}, followed by incubation at room temperature in the dark for approximately 5 min and fully washed with PBS immediately prior to analysis. The preparation of single cell suspension of biofilms was in consistent with protocol of Foladori et al. (2007).[16]

For the ALD, according to the previous study,[13] we employed a FITC-conjugated

peptide pan-caspase inhibitor, Z-VD-FMK, to detect if TiO_2-NPs-induced stress the expression of proteins that were capable of binding to caspase substrate peptides. Intracellular fluorescence, monitored by flow cytometry, is therefore indicative of stable binding of FITC-Z-VD-FMK to bacterial proteins with affinity for a general caspase substrate, and an increase in fluorescence reflects an increase in the concentration of these bacterial proteins. Further, we observed an increase in mean fluorescence at 24 hours for these treatments, revealing that the concentration of any caspase-like protein was increasing in response to prolonged and potentially overwhelming TiO_2-NPs-induced stress (Fig. 2A and 2B).

Confocal laser scanning microscopy (CLSM)

At the end of the experiment, the cell viability was assessed according to the depth of TiO_2-NPs penetrating into organisms. The live/dead staining procedure was performed according to the manufacturer's instructions. The kit provides a two-color fluorescence assay of bacterial viability relying on membrane integrity. The viable bacteria are stained by SYTO® 9 and fluoresce green, whereas the damaged bacteria are stained by propidium iodide and fluoresce red. At the end of the experiments, each sample was stained using the pre-mixed solution (SYTO 9 dye/propidium iodide/filtered-sterilized dH_2O=10-μL:10-μL:1-mL) available in the BacLight live/dead bacterial viability kits (Invitrogen). The original floc structure was observed under a confocal laser scanning microscope (Nikon A1, Japan), and ten random fields under each condition (with or without exposure to the TiO_2-NPs) were analyzed.

Test. S4. Calculation of the IBR

To address the biomarkers (the AEA in this study) as a whole, a general stress index termed the Integrated Biomarker Response (IBR) described by Beliaeff and Burgeot (2002)[17] was calculated. The procedure for IBR calculation of each biomarker response data is first standardized as Eq. (1):

$$Y_i = \frac{X_i - m}{s} \qquad Eq.\ (1)$$

where Y_i is the standardized value of the biomarker, X_i is the mean value of a biomarker at each time point, and *m* and *s* are the mean value and standard deviation of a biomarker considering all the samples of different time points, respectively.

Then Z_i defined as the absolute value of Y_i was computed as $Z_i = Y_i$ or $Z_i = -Y_i$, in the case of a biomarker was activated or inhibited by contaminations, respectively, and the minimum value (min_i) for each biomarker at all time points was obtained and added to Z_i. After these, the score of each biomarker response (S_i) was calculated as:

$$S_i = Z_i + |min_i| \qquad Eq.\ (2)$$

Finally, to achieve an integrated multi-biomarker response, star plots were used to display score results. The area A_i and corresponding IBR value were computed as:

$$A_i = \frac{S_i}{2} sin\alpha \left(S_i cos\beta + S_{i+1} sin\beta\right),\ \beta = arctan\left(\frac{S_{i+1} sin\alpha}{S_i - S_{i+1} cos\alpha}\right) \qquad Eq.\ (3)$$

$$IBR = \sum_{i=1}^{n} A_i \qquad Eq.\ (4)$$

where α is the angle between two adjacent lines, S_i and S_{i+1} represent two consecutive clockwise scores (radius coordinates) of the given star plot (Fig. 4).

Test. S5. TiO_2-NPs inhibition based on oxygen microprofiles

In accordance with the mass balance in the biofilm, derived using diffusion reaction kinetics, the net specific O_2 respiratory rate and NH_4^+ consumption (i.e., nitrification) rates are calculated using Fick's second law of diffusion with a consumption term. Due to the reasonably long interval between the adjacent points of measurement, we assumed that the O_2 and NH^{4+} microprofiles selected for analysis did change slightly.

$$R(z) = De\frac{d^2C_z}{dz^2} \qquad Eq.\ (5)$$

where $C(z, t)$ is the concentration at time t and depth z, and De is the effective diffusion coefficient in the biofilm, assuming that the molecular diffusion coefficients used for the calculations were 2.09×10^{-5} cm^2/s for O_2 and 1.38×10^{-5} cm^2/s for NH^{4+} at 20°C.[18] *R(z)* denotes the net specific metabolic rate namely, net specific O_2 respiration and NH^{4+} consumption (i.e., nitrification) rates at depth z. The differential solver supplied by the Origin software was used to obtain the second-order derivative of the O_2 profiles, enabling depiction of the net specific metabolic rates as they varied with depth.[19]

Inhibition ratios of O_2 respiration and nitrification activities in the biofilms were calculated from the following equation:

$$I = 1 - \frac{\sum R_T}{\sum R_U} \qquad Eq.\ (6)$$

where I is the inhibition ratio of the microbial activity in the biofilm. $\sum R_T$ is the total metabolic rate of the biofilm treated with TiO_2-NPs and $\sum R_U$ is the total metabolic

rate of the untreated biofilm.

Test. S6. Fluorescence in situ hybridization (FISH)

The following oligonucleotide probes, EUBMIX (containing EUB338, EUB338-II and EUB338-III, specific for most *Bacteria*), Nso190 and Nso1225 (specific for ammonia-oxidizing *Betaproteobacteria*), and Cren537 and Cren499 (specific for ammonia-oxidizing Archaea (AOA), *Crenarchaeaota*) were used for hybridization and listed in Table S3 (Supporting Information) according to the previous publication.[20, 21]

After exposure experiment, biofilms obtained from each carrier were fixed with freshly prepared 4% paraformaldehyde for 8 h at 4℃. After rinsing with phosphate buffer (pH 7.2), 10 μL of samples were immobilized on gelatin coated glass slide, dehydrated in the ethanol serials (50%, 80%, 90% and 100%, 5 min per step), and finally dried in air. Hybridization on the slide glass was performed according to the modified method.[20] Briefly, 20 μL of hybridization buffer (containing 0.9 M NaCl, 20 mM Tris-HCl (pH 7.2), 0.01% sodium dodecyl sulfate, 45% deionized formamide and 0.2 ng probes) was hybridized with the fixed samples, and then the slides were incubated in a prewarmed Boekel InSlide Out Hybridization Oven (Boekel Scientific, USA) at 46 ℃ for 2 h, followed by a washing step at 48 ℃ for 20 min in a washing buffer (20mM Tris-HCl (pH 7.2), 70 mM NaCl, 5 mM EDTA and 0.01% SDS). The washing buffer was removed by rinsing with sterile water and the slide was dried in air. A confocal laser scanning microscope (Nikon, Japan) equipped with an Ar ion laser (488 nm) and a He-Ne laser (543 nm) was used to detect and record probe-stained cells.

All image combining, processing, and analysis were performed with the standard software package provided by Zeiss.

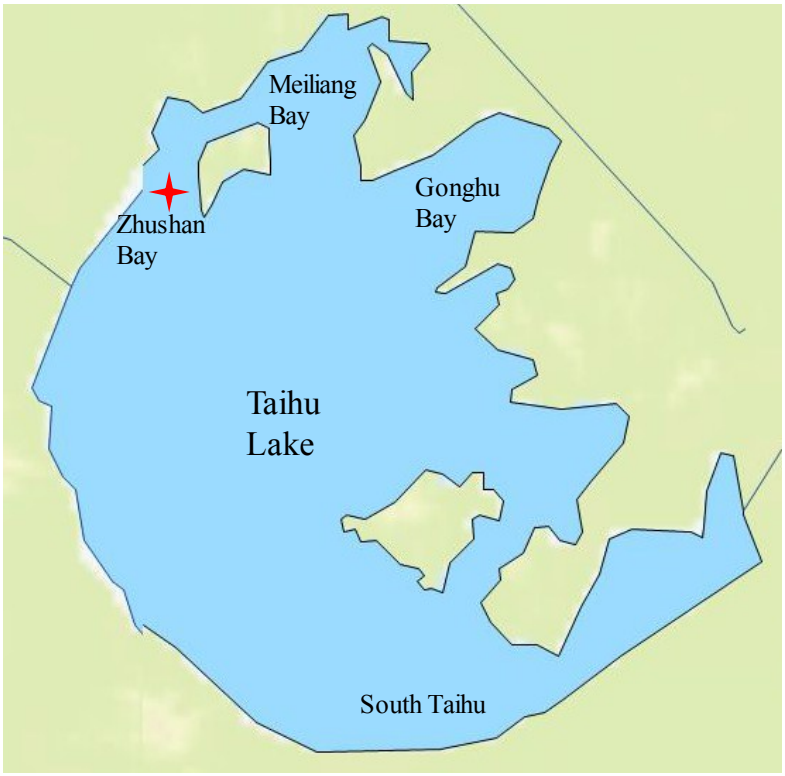

Fig. S1. The diagram of the sampling point in this study, and the asterisk (red) in the Zhushan Bay (31.3794 N, 120.0249 E) represents the sampling site of the biofilms (incubation and colonization) and lake water.

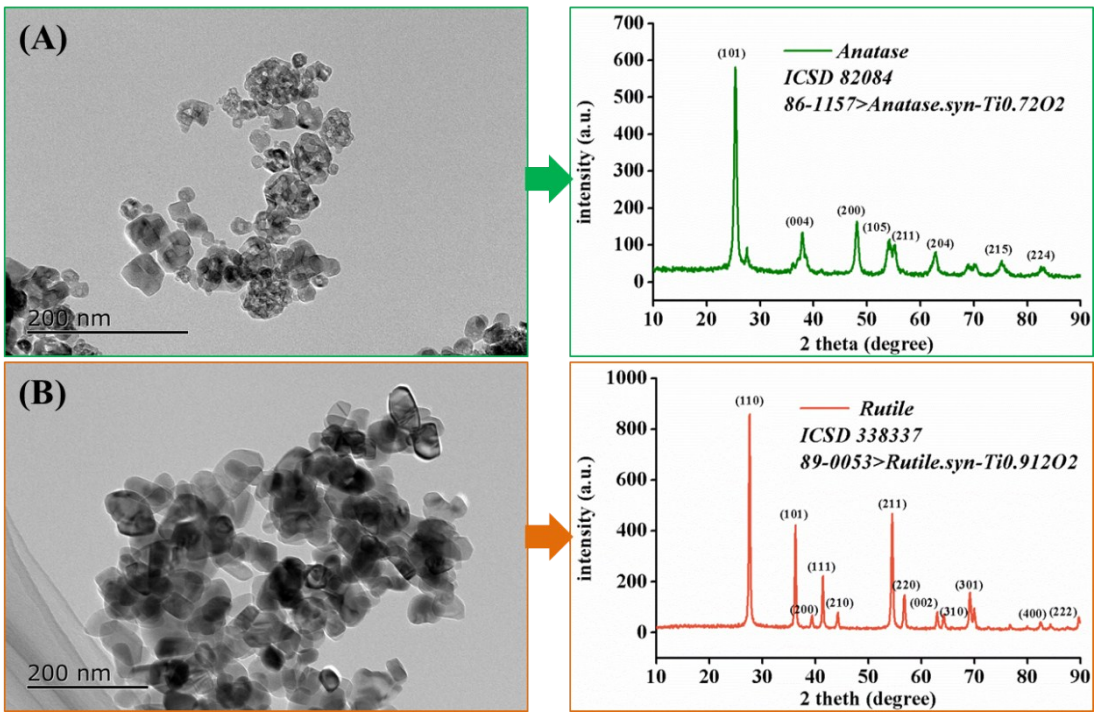

Fig. S2. TEM images and X-Ray diffraction pattern of two TiO_2-NPs.

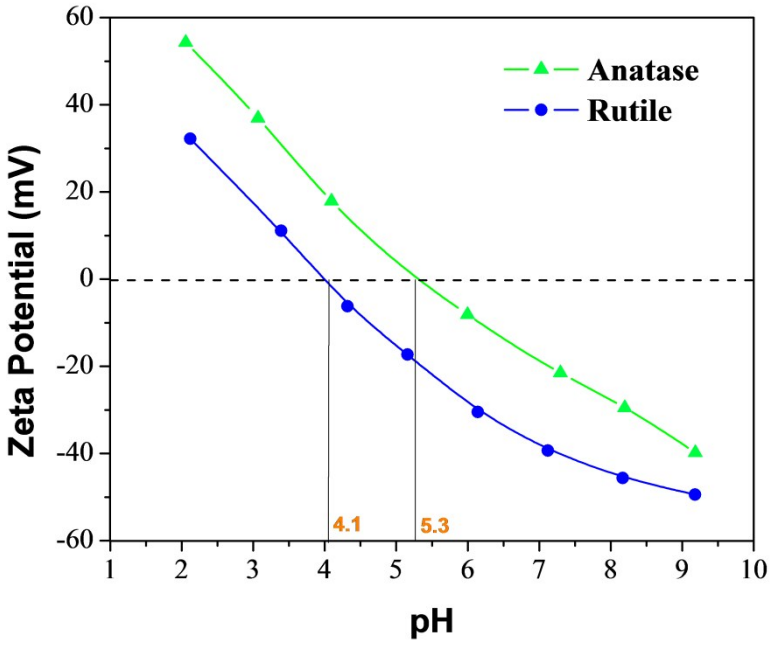

Fig. S3. The zeta potential of two TiO_2-NPs in Milli-Q water was measured from acid to alkaline and zero points of charge (pH_{zpc}).

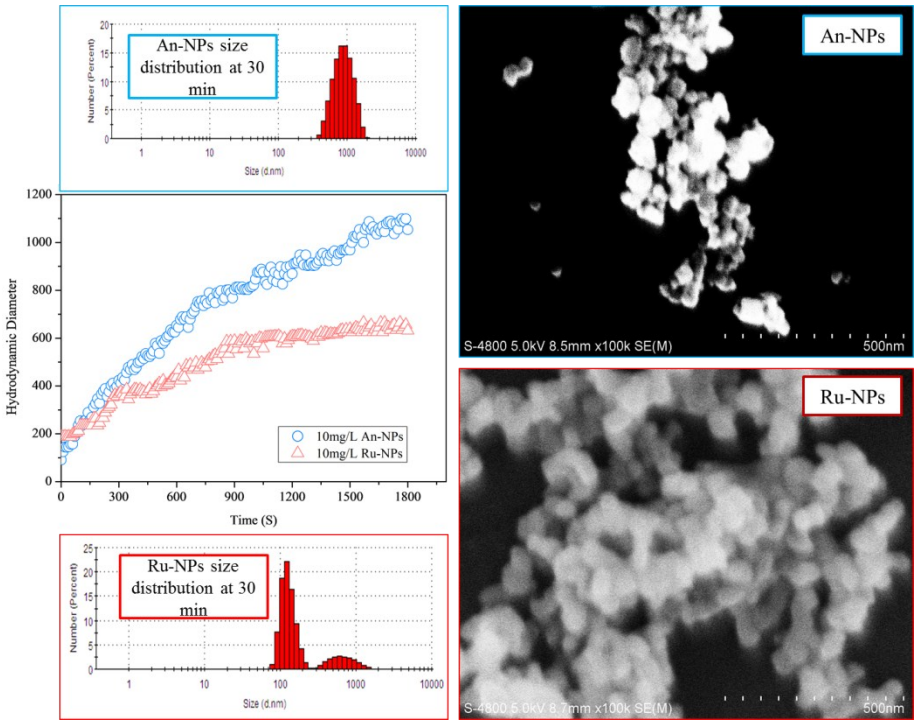

Fig. S4. Aggregation of An-NPs and Ru-NPs in the filtered lake-water (through 0.22 μm). The aggregation kinetics of TiO_2-NPs were measured in the first at 30 min and size distributions of TiO_2-NPs were also determined at the 30 min. The figures on the right represent the SEM images of nano-aggregates.

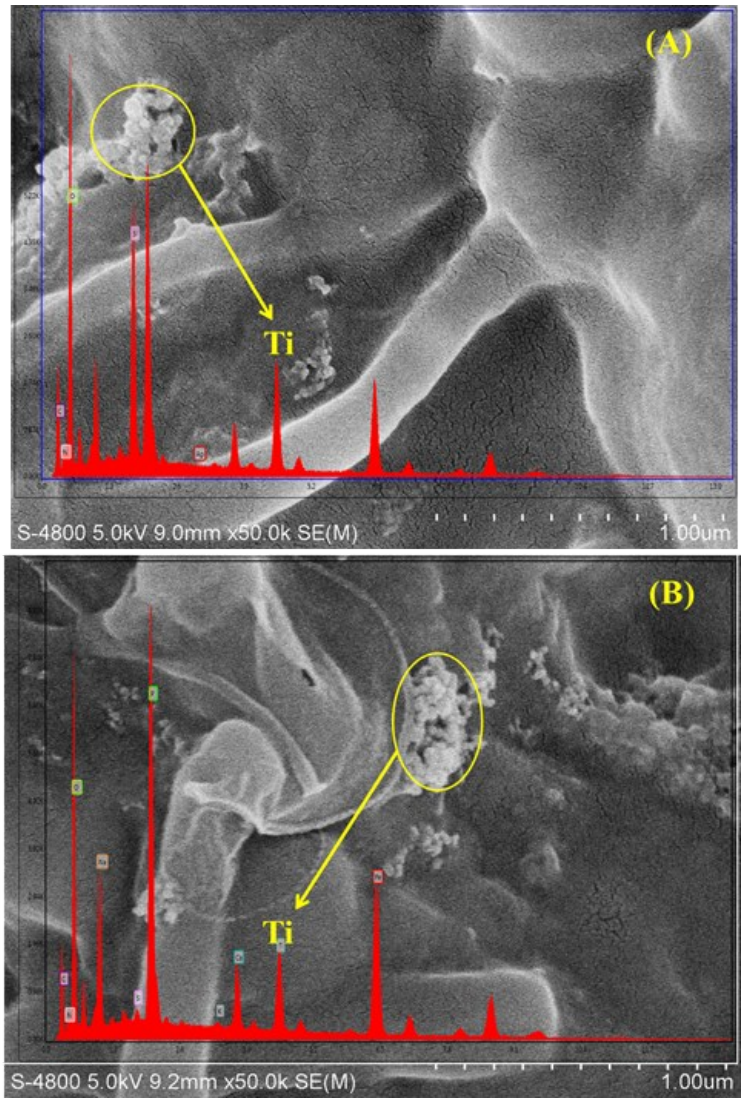

Fig. S5. SEM images and energy dispersive spectrometer (EDS) of biofilm after bio-sorption for An-NPs (A) and Ru-NPs (B) with concentration of 10 mg L^{-1}.

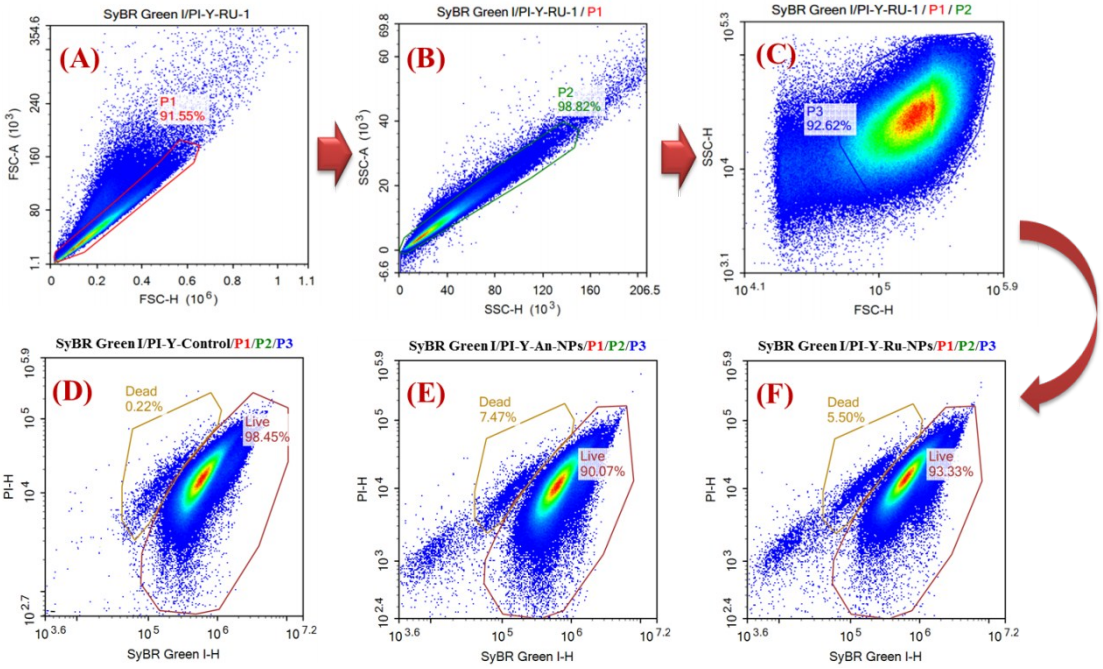

Fig. S6. The live and dead bacterial cells (NLD) in biofilms exposed to two TiO_2-NPs based on the integrity of cell membrane. Red versus green fluorescence cytogram for biofilms cells stained with SYBR Green I and PI. (A) and (B) and (C) the removal of adhesions and impurities ; (D) Control; (E) 10 mg L^{-1} An-NPs; (F) 10 mg L^{-1} Ru-NPs.

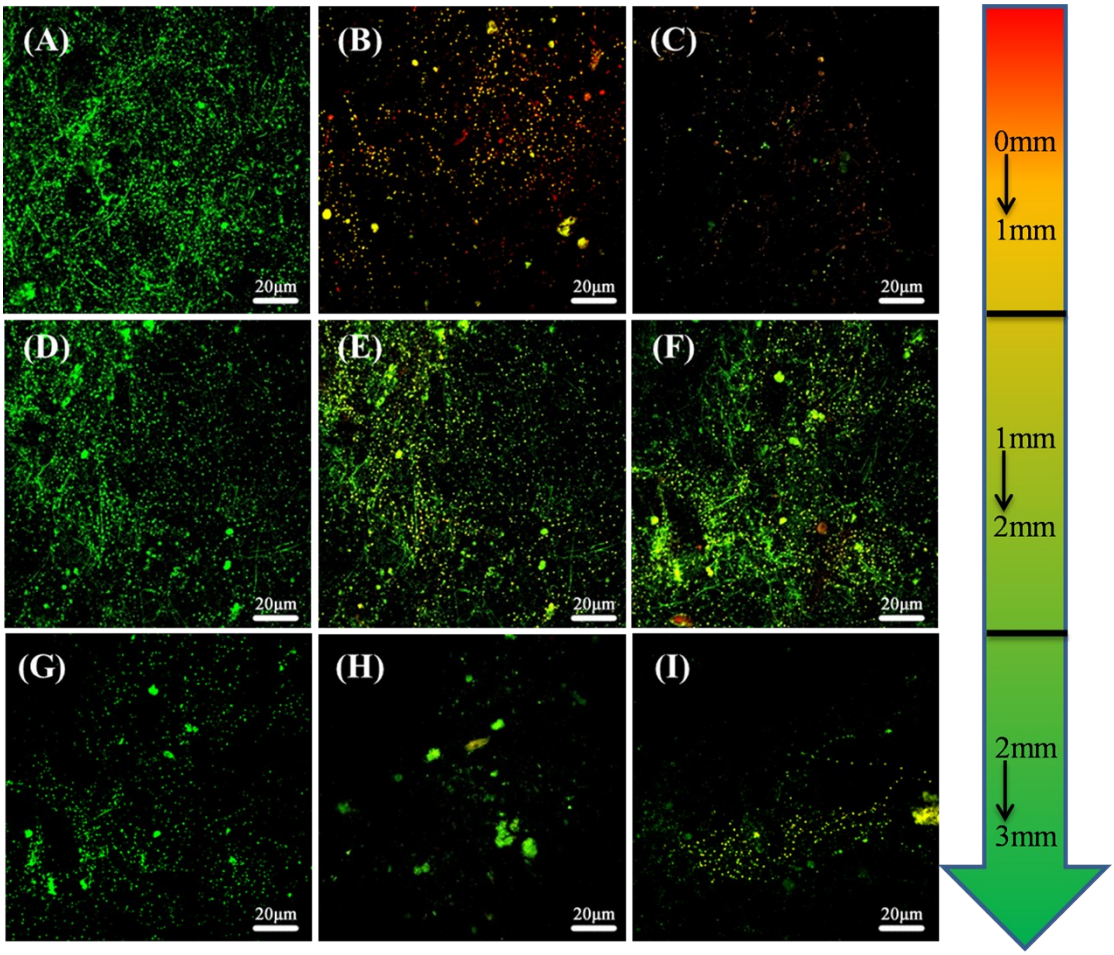

Fig. S7. CLSM images of bacterial and algae activities in freshwater biofilms at different thicknesses at the end of the experiment. Control: (A), (D), and (G); 10 mg L^{-1} An-NPs: (B), (E), and (H); 10 mg L^{-1} Ru-NPs: (C), (F), and (I).

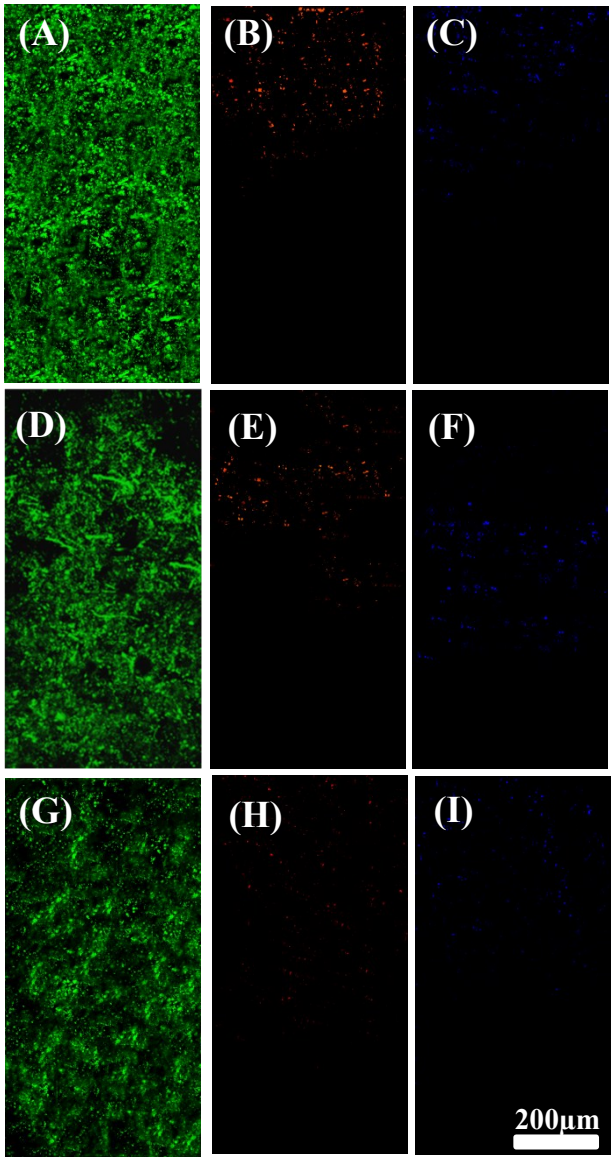

Fig. S8. Fluorescence in situ hybridization (FISH) images showing the in situ spatial distributions of heterotrophic bacteria, ammonia-oxidizing Betaproteobacteria (AOB) and Crenarchaeaota, ammonia-oxidizing Archaea (AOA) in the biofilms. (A) Control, (D) An-NPs, and (G) Ru-NPs: FISH with cyanine (Cy-5)-labeled probe EUBmix (EUB338, EUB338-II, and EUB338-III). (B) Control, (E) An-NPs, and (H) Ru-NPs: FISH with cyanine (Cy-3)-labeled probe Nso190 and Nso1225. (C) Control, (F) An-NPs, and (I) Ru-NPs: FISH with 4´,6-diamidino-2-phenylindole (DAPI)-labeled probe Cren537 and Cren499. Scale bar for all images = 200 µm. The biofilm surface is the top of the image. Note: Fig. S8 provides replicate for the FISH results presented in Fig. 6 since bacterial distribution in the biofilms are heterogeneous.

Table S1. Characterization of the filtered lake water (through 0.22 μm) sampled from the Zhushan Bay of Lake Taihu, China.

Parameters	Average values (n=5)
TOC ($mg \cdot L^{-1}$)	10.78±3.8
pH	7.26±0.8
K^+ ($mg \cdot L^{-1}$)	4.23±0.5
Na^+ ($mg \cdot L^{-1}$)	32.3±2.1
Ca^{2+} ($mg \cdot L^{-1}$)	33.4±3.1
Mg^{2+} ($mg \cdot L^{-1}$)	7.59±1.8
PO_4^{3-} ($mg \cdot L^{-1}$)	<0.046
SO_4^{2-} ($mg \cdot L^{-1}$)	56.2±3.0
Cl^- ($mg \cdot L^{-1}$)	42.4±2.4
HCO_3^- ($mg \cdot L^{-1}$)	95.6±3.7
CO_3^{2-} ($mg \cdot L^{-1}$)	<1.78
NO_3^- ($mg \cdot L^{-1}$)	1.15±0.3
NH_4^+ ($mg \cdot L^{-1}$)	0.387±0.2

Table S2. Nutrients concentration of cultivation medium

Element	Reagent	Concentration (Reagent, μM)
C	$C_6H_{12}O_6$	200
N	NH_4Cl	25
N	$NaNO_3$	55
K, P	Na_2HPO_4, KH_2PO_4	32, 60
Ca	$CaCl_2$	100
Mg	$MgCl_2 \cdot 6H_2O$	50
Cu	$CuSO_4 \cdot 5H_2O$	2
Mn	$MnCl_2 \cdot 4H_2O$	2
Fe	$FeCl_2$	80
Zn	$ZnSO_4 \cdot 7H_2O$	0.07

Table S3. Oligonucleotide probes used in this study

Probe	Sequence 5'-3'	Formamide (%)	Specificity
EUB338	GCTGCCTCCCGTAGGAGT	45	Most *Bacteria* [22]
EUB338-II	GCAGCCACCCGTAGGTGT	45	*Planctomycetales* and other *Bacteria* [22]
EUB338-III	GCTGCCACCCGTAGGTGT	45	*Verrucomicrobiales* and other *Bacteria* [22]
AOB-Nso190	CGATCCCCTGCTTTTCTCC	45	AO-*Betaproteobacteria* [20]
AOB-Nso1225	CGCGATTGTATTACGTGTGA	45	AO-*Betaproteobacteria* [20]
AOA-Cren537	TGACCACTTGAGGTGCTG	45	*Crenarchaeaota* [23]
AOA-Cren499	CCAGRCTTGCCCCCCGCT	45	*Crenarchaeaota* [24]

.

References

1. Y. Xu, C. Wang, J. Hou, S. Dai, P. Wang, L. Miao, B. Lv, Y. Yang and G. You, Effects of ZnO nanoparticles and Zn2+ on fluvial biofilms and the related toxicity mechanisms, *Science Of the Total Environment*, 2016, **544**, 230-237.

2. K. Li, J. Qian, P. Wang, C. Wang, J. Liu, X. Tian, B. Lu and M. Shen, Crystalline phase-dependent eco-toxicity of titania nanoparticles to freshwater biofilms, *Environmental Pollution*, 2017, **231**, 1433-1441.

3. H. Schug, C. W. Isaacson, L. Sigg, A. A. Ammann and K. Schirmer, Effect of TiO2 nanoparticles and UV radiation on extracellular enzyme activity of intact heterotrophic biofilms, *Environmental Science & Technology*, 2014, **48**, 11620-11628.

4. J. Hou, G. You, Y. Xu, C. Wang, P. Wang, L. Miao, S. Dai, B. Lv and Y. Yang, Antioxidant enzyme activities as biomarkers of fluvial biofilm to ZnO NPs ecotoxicity and the Integrated Biomarker Responses (IBR) assessment, *Ecotoxicology and Environmental Safety*, 2016, **133**, 10-17.

5. L. Miao, W. Chao, J. Hou, P. Wang, Y. Ao, L. Yi, B. Lv, Y. Yang, G. You and X. Yi, Effect of alginate on the aggregation kinetics of copper oxide nanoparticles (CuO NPs): bridging interaction and hetero-aggregation induced by Ca 2+, *Environmental Science & Pollution Research*, 2016, **23**, 1-9.

6. J. Qian, K. Li, P. Wang, C. Wang, J. Liu, X. Tian, B. Lu and W. Guan, Unraveling adsorption behavior and mechanism of perfluorooctane sulfonate (PFOS) on aging aquatic sediments contaminated with engineered nano-TiO2, *Environmental science and pollution research international*, 2018, DOI: 10.1007/s11356-018-1984-4.

7. S. Jomini, H. Clivot, P. Bauda and C. Pagnout, Impact of manufactured TiO2 nanoparticles on planktonic and sessile bacterial communities, *Environmental Pollution*, 2015, **202**, 196-204.

8. B. Chu Thi Thanh, T. Tong, J.-F. Gaillard, K. A. Gray and J. J. Kelly, Acute Effects of TiO2 Nanomaterials on the Viability and Taxonomic Composition of Aquatic Bacterial Communities Assessed via High-Throughput Screening and Next Generation Sequencing, *Plos One*, 2014, **9**.

9. S. Bao, H. Wang, W. Zhang, Z. Xie and T. Fang, An investigation into the effects of silver nanoparticles on natural microbial communities in two freshwater sediments, *Environmental Pollution*, 2016, **219**, 696-704.

10. G. Nebevoncaron, P. J. Stephens, C. J. Hewitt, J. R. Powell and R. A. Badley, Analysis of bacterial function by multi-colour fluorescence flow cytometry and single cell sorting, *Journal of Microbiological Methods*, 2000, **42**, 97-114.

11. K. Li, J. Qian, P. Wang, C. Wang, X. Fan, B. Lu, X. Tian, W. Jin, X. He and W. Guo, Toxicity of Three Crystalline TiO2 Nanoparticles in Activated Sludge: Bacterial Cell Death Modes Differentially Weaken Sludge Dewaterability, *Environmental science & technology*, 2019, **53**, 4542-4555.

12. A. Hochman, Programmed Cell Death in Prokaryotes, *Critical Reviews in Microbiology*, 1997,

23, 207-214.

13. D. J. Dwyer, D. M. Camacho, M. A. Kohanski, J. M. Callura and J. J. Collins, Antibiotic-Induced Bacterial Cell Death Exhibits Physiological and Biochemical Hallmarks of Apoptosis, *Molecular Cell*, 2012, **46**, 561-572.

14. S. Barbesti, S. Citterio, M. Labra, M. D. Baroni, M. G. Neri and S. Sgorbati, Two and three-color fluorescence flow cytometric analysis of immunoidentified viable bacteria, *Cytometry*, 2015, **40**, 214-218.

15. M. G. Weinbauer, C. Beckmann and M. G. Hofle, Utility of green fluorescent nucleic acid dyes and aluminum oxide membrane filters for rapid epifluorescence enumeration of soil and sediment bacteria, *Applied And Environmental Microbiology*, 1998, **64**, 5000-5003.

16. P. Foladori, B. Laura, A. Gianni and Z. Giuliano, Effects of sonication on bacteria viability in wastewater treatment plants evaluated by flow cytometry - Fecal indicators, wastewater and activated sludge, *Water Research*, 2007, **41**, 235-243.

17. B. Beliaeff and T. Burgeot, Integrated biomarker response: A useful tool for ecological risk assessment, *Environmental Toxicology And Chemistry*, 2002, **21**, 1316-1322.

18. S. Hisashi, S. Yuichi, N. Yoshiyuki, O. Satoshi and S. Takuya, Use of microelectrodes to investigate the effects of 2-chlorophenol on microbial activities in biofilms, *Biotechnology & Bioengineering*, 2005, **91**, 133-138.

19. J. Hou, L. Miao, C. Wang, P. Wang, Y. Ao, J. Qian and S. Dai, Inhibitory effects of ZnO nanoparticles on aerobic wastewater biofilms from oxygen concentration profiles determined by microelectrodes, *Journal of Hazardous Materials*, 2014, **276**, 164-170.

20. X. Zheng, Y. Chen and R. Wu, Long-Term Effects of Titanium Dioxide Nanoparticles on Nitrogen and Phosphorus Removal from Wastewater and Bacterial Community Shift in Activated Sludge, *Environmental Science & Technology*, 2011, **45**, 7284-7290.

21. S. Hisashi, S. Yuichi, N. Yoshiyuki, O. Satoshi and S. Takuya, Use of microelectrodes to investigate the effects of 2-chlorophenol on microbial activities in biofilms, *Biotechnology & Bioengineering*, 2010, **91**, 133-138.

22. Z. Ji and Y. Chen, Using Sludge Fermentation Liquid To Improve Wastewater Short-Cut Nitrification-Denitrification and Denitrifying Phosphorus Removal via Nitrite, *Environmental Science & Technology*, 2010, **44**, 8957-8963.

23. E. Teira, T. Reinthaler, A. Pernthaler, J. Pernthaler and G. J. Herndl, Combining catalyzed reporter deposition-fluorescence in situ hybridization and microautoradiography to detect substrate utilization by bacteria and archaea in the deep ocean, *Applied And Environmental Microbiology*, 2004, **70**, 4411-4414.

24. C. M. Fitzgerald, P. Comejo, J. Z. Oshlag and D. R. Noguera, Ammonia-oxidizing microbial communities in reactors with efficient nitrification at low-dissolved oxygen, *Water Research*, 2015, **70**, 38-51.